Fizika Nizkikh Temperatur, 2000, v. 26, Nos. 9/10, p. 889–898

Observation of the high resolution infrared absorption spectrum of CO_2 molecules isolated in solid parahydrogen

Simon Tam and Mario E. Fajardo

Propulsion Directorate, U.S. Air Force Research Laboratory AFRL/PRSP, Bldg. 8451, Edwards AFB, CA 93524–7680
E-mail: mario_fajardo@ple.af.mil

Received February 17, 2000, revised May 4, 2000

We report the observation of high resolution (0.008 cm^{-1}) infrared absorption spectra of CO_2 molecules isolated in solid parahydrogen (pH_2) matrices at $T = 2.4$ to 4.8 K. Several extremely sharp (0.01 to 0.04 cm^{-1} full-width-at-half-maximum) absorption features appear in the 2343.5 to 2345 cm^{-1} region. We assign the three strongest peaks to the ν_3 mode of isolated CO_2 molecules. The spectra are consistent with trapping of the CO_2 molecules in three distinct double-substitutional sites in hcp and fcc regions of the pH_2 solid. We offer several hypotheses as to the origins of the numerous weaker absorption features.

PACS: 07.20.Mc, 61.72.Ww, **67.80.–s**, **78.30.–j**, 81.10.Bk, 81.30.Kf

1. Introduction

This manuscript is a status report on our continuing effort to observe and analyze vibrational spectra of molecular dopants isolated in cryogenic solid parahydrogen (pH_2) hosts. As detailed below, our investigation of the microscopic structures and dynamics underlying many of these spectra is at a preliminary stage. Despite this, we believe the experimental observations themselves merit being reported at this time. We hope that these new high-resolution data will stimulate interest in the rigorous testing of theoretical models of vibrational spectroscopy of impurities in condensed phases.

The suitability of solid pH_2 as a host for high-resolution ($\Delta\nu/\nu \sim 10^{-6}$) vibrational spectroscopy was discovered by Oka and co-workers [1–5], and further investigated by Shida, Momose and co-workers [6–10], and by Winnewisser and co-workers [11–14]. The favorable properties of solid pH_2 contributing to this phenomenon have been discussed in detail [2,3,9]. Here we note simply that solid pH_2 is very «forgiving» of highly non-equilibrium sample preparation techniques such as direct gas-to-solid condensation. Structural defects in such samples may be less numerous, and/or have a smaller influence on dopant vibrational spectra, than in other vapor deposited cryogenic van der Waals solids traditionally employed as hosts for matrix isolation spectroscopy (MIS).

Our work on solid pH_2 is supported by the U.S. Air Force's High Energy Density Matter (HEDM) program [15]; our project's ultimate objective is to demonstrate practical energy storage in cryogenic solids for use as advanced chemical rocket propellants. Thus, our attention is focused on the problems of (a) trapping large concentrations of isolated energetic dopants, (b) scaling-up sample quantities beyond the thin films typically encountered in MIS studies, (c) rigorously characterizing the chemical identities, concentrations, and trapping site structures of the incorporated energetic species, and (d) evaluating the thermal and chemical stabilities of these prototypical «cryosolid» propellants. These last two tasks motivate our interest in the spectroscopy of dopants in solid pH_2 .

Our new «rapid vapor deposition» technique produces easily doped, millimeters-thick pH_2 solids of remarkable optical clarity [16,17]. The compatibility of this method with most MIS dopant trapping schemes enables the isolation in solid pH_2 of a wide variety of previously inaccessible chemical species. The excellent transparency of rapid vapor deposited samples is unusual for pH_2 solids produced by vapor deposition onto a substrate-in-va-

© Simon Tam and Mario E. Fajardo, 2000

cuum [18], and enables their characterization by optical methods.

Our early work on doped cryogenic hydrogen solids employed medium-resolution ultraviolet/visible and infrared (IR) diagnostics [19–21]. However, we recently added a high-resolution IR capability and were repaid by the observation of very sharp (~ 0.01 cm^{-1} full-width-at-half-maximum, FWHM) vibrational absorption features for dopants in rapid vapor deposited samples. Moreover, high-resolution IR spectra of several (presumably) simple molecular dopants in solid $p\mathrm{H}_2$ exhibit amazingly rich structure. Not only are the vibrational transition energies often more precisely defined than for the same dopants in rare gas solid (RGS) hosts, but such spectra also typically include a larger number of distinct, well resolved features. The increased precision and complexity of these spectral measurements may require extraordinary efforts for their complete assignment, but the reward should be a deeper and more quantitative understanding of dopant trapping site structures and vibrational dynamics in solid $p\mathrm{H}_2$ than has been achieved to date by MIS in RGS hosts.

We are in the process of surveying high-resolution IR absorption spectra for a variety of dopants in solid $p\mathrm{H}_2$. A substantial database of such spectra should help to determine which physical effects dominate the vibrational spectroscopy of different classes of dopants in solid $p\mathrm{H}_2$. For example, spectra of $\mathrm{CH}_4/p\mathrm{H}_2$ solids [6,7,9,10,22], a case in which the spherical-top dopant fits easily into a single-substitutional trapping site, accordingly show line spacings and intensity progressions commensurate with slightly hindered rotors [6,22–27]. Structurally, the spectra demonstrate that in as-prepared rapid vapor deposited $p\mathrm{H}_2$ solids some of the CH_4 molecules are initially trapped in face-centered-cubic (fcc) regions, and that these regions convert irreversibly to hexagonal-close-packed (hcp) upon annealing [22]. The polarization dependences of the $\mathrm{CH}_4/p\mathrm{H}_2$ transitions further indicate that annealing also results in improved alignment of the hcp crystallites' c-axis orientations with the deposition substrate surface normal [22]. Dynamically, all the $\mathrm{CH}_4/p\mathrm{H}_2$ spectra can be rigorously assigned by considering the rotational-vibrational dynamics of CH_4 at the center of static external fields having D_{3h} [6] and O_h [22] symmetries. Thus, a satisfactory explanation of these transition energies does not require consideration of constrained rotational-translational-coupling (RTC) in a rigid trapping site [28–31], or of more general RTC interactions within a dynamic trapping site structure [32–37]. These lessons learned from the $\mathrm{CH}_4/p\mathrm{H}_2$ studies provide an excellent starting point for the assignment of our recently observed highly structured $\mathrm{CO}/p\mathrm{H}_2$ spectra [38], another case in which the dopant molecule should fit readily into a single substitutional vacancy.

In stark contrast, we find that spectra of many larger species, such as lower symmetry polyatomic molecules, and hydrogen- or van der Waals-bonded clusters of smaller dopant molecules, show no evidence of overall rotation. We believe end-over-end rotation is inhibited by strong anisotropic interactions within the lower symmetry multi-substitutional trapping sites required to accommodate such large species. Thus, these larger species likely exist in the «librational» limit, oscillating around certain equilibrium orientations instead of rotating as a unit [23]. Yet, despite such strong dopant-host interactions, many of these larger dopant systems exhibit even sharper vibrational absorptions than those observed for smaller dopants trapped in highly symmetrical single substitutional sites! A satisfactory analysis of the spectra of these larger librating systems must deal with the additional complication of simultaneously considering both inherent and trapping-site-induced spectral features.

Before attempting such analyses, we turn first to a simpler model system of a linear triatomic molecule such as CO_2 in solid $p\mathrm{H}_2$. Our IR spectra of $\mathrm{CO}_2/p\mathrm{H}_2$ samples show complicated patterns of sharp lines which do not appear to match a rotational dynamics (*vide infra*), and so may be comparable in this respect to the larger dopants. However, the gas-phase vibrational transitions of CO_2 are very well known; thus, any peculiar features in spectra of $\mathrm{CO}_2/p\mathrm{H}_2$ are immediately attributable to either dopant-dopant interactions or to interactions with the $p\mathrm{H}_2$ host. We think the $\mathrm{CO}_2/p\mathrm{H}_2$ system will prove to be an excellent arena for evaluating the various elements of the RTC models in the limit of strongly hindered rotation.

In what follows we describe briefly our experimental methods and present our preliminary high-resolution IR absorption data for the $\mathrm{CO}_2/p\mathrm{H}_2$ system. We will show that the strongest absorption features are due to isolated CO_2 molecules, and not to $(\mathrm{CO}_2)_n$ clusters. We discuss these monomer spectra in terms of candidate trapping site structures, and the corresponding rotational vs librational dynamics of the trapped molecules. We will give a list of hypotheses about the possible origins of the numerous weaker absorption features, but attempt no quantitative application of crystal field

or RTC models at this time. We end this manuscript with a summary, and list some of our immediate plans for future experimental and theoretical work to test the proposed hypotheses.

2. Experimental

Our experimental apparatus and sample preparation techniques have been described in detail before [16,17,21]. Doped pH_2 solids are prepared by rapid vapor deposition of precooled pH_2 gas and room temperature CO_2 gas onto a BaF_2 substrate cooled to $T \approx 2$ K in a liquid helium (lHe) bath cryostat. We operate the ortho/para hydrogen converter at 15 K, yielding a flow of pre-cooled pH_2 containing $\approx 0.01\%$ residual orthohydrogen (oH_2) impurities [17]. The pH_2 flow impinges upon the substrate at a 45° angle; during a deposition the pressure of uncondensed pH_2 gas remains below $\sim 10^{-4}$ Torr. The CO_2 dopant is metered into the deposition cryostat from a separate gas handling manifold; the dopant inlet is situated at an angle of 45° from the substrate surface normal, at 90° to the pH_2 source. Individual sample preparation details are given below in the figure captions.

We record IR absorption spectra of our CO_2/pH_2 samples across the 800 to 7800 cm^{-1} range at a resolution of 0.008 cm^{-1}; the main optical axis is parallel to the substrate normal. The Fourier transform IR spectrometer (Bruker IFS120HR) is equipped with a glowbar source, a KBr beamsplitter, and a liquid nitrogen cooled HgCdTe detector. To accommodate the IR diagnostic, the entire optical path is enclosed within a 0.5 m^3 polycarbonate box purged with a constant flow of dry N_2 gas.

3. Results

Figure 1 shows the ν_3 $^{12}C^{16}O_2$ region of absorption spectra from three different as-deposited pH_2 solids containing CO_2 concentrations ranging from ~ 0.01 ppm up to 1.2 ppm. The concentrations are

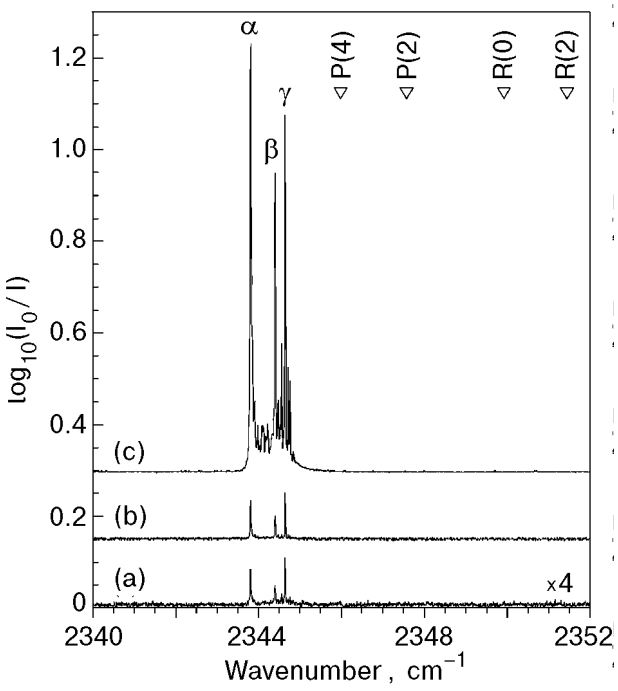

Fig. 1. IR absorption spectra of three as-deposited pH_2 solids at $T = 2.4$ K containing different concentrations of natural isotopic abundance CO_2 . Trace (1a) is for a 13 ppm CO/pH_2 sample containing ~ 0.01 ppm CO_2 as an unintentional impurity; sample thickness is 2.7 mm. Trace (1b) is for an 8 ppm HCl/pH_2 sample containing ≈ 0.04 ppm CO_2 as an unintentional impurity; sample thickness is 3.0 mm. Trace (1c) is for a 1.2 ppm CO_2/pH_2 sample that is 1.4 mm thick. The inverted triangles at the top of the figure indicate the positions of several gas phase ro-vibrational lines for the ν_3 mode of $^{12}C^{16}O_2$ [40]. Trace (1a) has been rescaled by a multiplicative factor of 4; all the traces have been displaced vertically for ease of presentation.

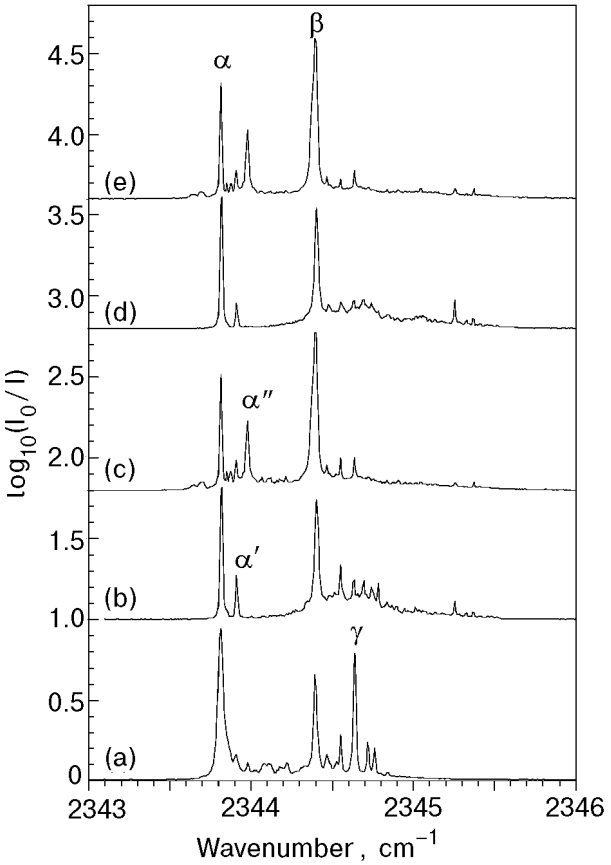

Fig. 2. Annealing behavior of the 1.2 ppm CO_2/pH_2 sample described in Fig. 1. Trace (2a) is an expanded view of the as-deposited spectrum presented above in trace (1c). The temperature sequence is: (2a) $T = 2.4$ K, (2b) $T = 4.8$ K, (2c) $T = 2.4$ K, (2d) $T = 4.8$ K, and (2e) $T = 2.4$ K. The labels α' and α'' denote two new features that grow in during annealing.

Table

Peak positions (cm^{-1}) and widths (FWHM, rounded to nearest 0.005 cm^{-1}), and assignments for the main IR absorptions in CO_2/pH_2. The labels α, β, and γ refer to the three largest peaks observed in as-deposited samples; the labels α′ and α″ refer to two additional strong features that appear between α and β upon temperature cycling. The «as-deposited» spectra are taken at $T = 2.4$ K, the «annealing» spectra at $T = 4.8$ K, and the «annealed» spectra upon re-cooling to $T = 2.4$ K. The gas-phase vibrational band origins, ν_0, are estimated from data in Ref. 40

Label	Peak positions (widths)			Assignment
	as-deposited	annealing	annealed	
α	2278.296 (0.040)	2278.300 (0.015)	2278.299 (0.010)	$\nu_3\ ^{13}C^{16}O_2$
α′		n.o.		$\nu_0 = 2283.48$
α″			2278.454w (0.025)	
β	2278.861 (0.030)	2278.872 (0.030)	2278.867 (0.025)	
γ	2279.099 (0.015)			
α	2326.835 (0.035)	2326.842 (0.015)	2326.842 (0.015)	$\nu_3\ ^{16}O^{12}C^{18}O$
α′		n.o.		$\nu_0 = 2332.11$
α″			n.o.	
β	2327.41w	2327.42w	2327.399 (0.010) 2327.422 (0.010)	
γ	2327.656 (0.020)			
α	2343.813 (0.040)	2343.818 (0.020)	2343.814 (0.015)	$\nu_3\ ^{12}C^{16}O_2$
α′		2343.912 (0.015)		$\nu_0 = 2349.14$
α″			2343.979 (0.020)	
β	2344.395 (0.025)	2344.404 (0.030)	2344.397 (0.040)*	
γ	2344.639 (0.020)			

w — weak, signal/noise ~ 1; n.o. — not observed, signal/noise < 1; * — shoulder at 2344.372 cm^{-1}.

estimated as described previously [21] using a value of 550 km/mol for the ν_3 CO_2 integrated absorption coefficient [39]. The peaks labeled α, β, and γ dominate all three spectra, but show minor sample-to-sample variations in relative intensities. Not shown are the $\nu_3\ ^{13}C^{16}O_2$ and $\nu_3\ ^{16}O^{12}C^{18}O$ regions of the spectrum depicted in trace (1c), in which similar features, also matrix-shifted by ≈ -5 cm^{-1} from the gas-phase vibrational band origins [40,41], appear for each natural abundance isotopomer. The observed peak positions and linewidths are summarized in the Table.

Figure 2 shows the effects of repeated temperature cycling on the $\nu_3\ ^{12}C^{16}O_2$ band of the 1.2 ppm CO_2/pH_2 sample depicted in trace (1c). The most pronounced change observed during the initial warming from $T = 2.4$ to 4.8 K is the strong irreversible decrease in the intensity of the γ peak at 2344.64 cm^{-1}; the same behavior is observed for the other CO_2 isotopomers, as well. We also note the simultaneous growth of the α′ peak at 2343.91 cm^{-1}, the weakening and sharpening of the α line, the strengthening and broadening of the β peak, and the appearance of a ≈ 0.5 cm^{-1} broad absorption lump near 2344.6 cm^{-1}. Trace (2c) shows that upon re-cooling to $T = 2.4$ K the α and α′ peaks weaken, a new α″ line appears at 2343.98 cm^{-1} together with other weaker features in the 2343.6 to 2343.9 cm^{-1} region, the β feature strengthens and broadens further, and the 2344.6 cm^{-1} lump broadens and/or diminishes. Repeating the temperature cycle, traces (2d) and (2e), shows the largely reversible nature of these changes. As reported in the Table, the broadening of the $\nu_3\ ^{12}C^{16}O_2$ β feature upon annealing is largely due to the appearance of a shoulder on the

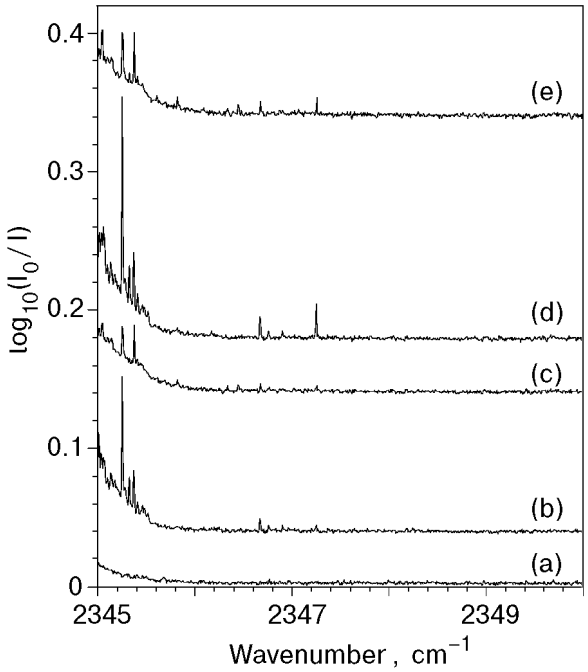

Fig. 3. Continuation of the spectra presented in Fig. 2.

red side of the main peak; the ν_3 $^{16}O^{12}C^{18}O$ β feature actually splits completely into two sharp, well-resolved peaks separated by ≈ 0.02 cm^{-1} .

Figure 3 shows the 2345 to 2350 cm^{-1} region of the same spectra as depicted in Fig. 2. Several sharp new peaks appear upon temperature cycling, most notably those near 2345.25, 2345.37, 2346.67, and 2347.25 cm^{-1} .

4. Discussion

4.1. Isolation of CO_2 *molecules*

We assign the α, β, and γ features to isolated CO_2 molecules as opposed to $(CO_2)_n$ clusters due to: (1) the extreme dilutions of the samples, (2) the lack of any systematic concentration dependence, and (3) the absence (for as-deposited CO_2/pH_2 solids) of any other absorption features outside a narrow ≈ 1 cm^{-1} window. Assessing the validity of this last point requires a brief review of the literature on $(CO_2)_n$ clusters.

The gas-phase vibrational band origin for the localized asymmetric stretch mode of «slipped parallel» CO_2 dimers is observed [42] to be shifted by +1.63 cm^{-1} relative to the monomer ν_3 $^{12}C^{16}O_2$ band origin at 2349.14 cm^{-1} ; theoretical calculations [43–45] predict shifts of between 0 and +2 cm^{-1} , depending on the dimer geometry. The cyclic C_{3h} symmetry CO_2 trimer band origin is shifted by +2.58 cm^{-1} [46], and the non-cyclic C_2 symmetry CO_2 trimer shows two bands with origins shifted by −5.85 cm^{-1} and +3.58 cm^{-1} [47], all shifts again referenced to the gas-phase monomer ν_3 band origin. Larger gas-phase $(CO_2)_n$ clusters [48] and ultra-fine particles [49] show broad absorptions across the 2340 to 2380 cm^{-1} range. The absorption maximum in pure, crystalline, natural isotopic abundance solid CO_2 occurs at 2344.8 cm^{-1}, but solid samples prepared by different methods can show absorptions anywhere between 2330 and 2380 cm^{-1} [50–53].

Matrix isolation studies involving general X–CO_2 complexes are far too numerous to list here exhaustively [54–56]. The IR absorption spectrum of a 1 ppm CO_2/N_2 solid carefully prepared from the melt shows a single sharp line with a width of ≈ 0.007 cm^{-1} at $T = 11$ K, which is assigned to librating CO_2 molecules isolated in single-substitutional sites [57]. All other previously reported ν_3 region spectra of solely CO_2 doped rare gas [58–62], deuterium [63,64], and pH_2 [65] matrices show multiple absorption features spanning a 5 to 10 cm^{-1} range. These features are preparation, concentration, and annealing dependent, and are assigned to CO_2 molecules in multiple trapping sites, and/or to aggregated $(CO_2)_n$ species. Most directly relevant to this discussion are the spectra of $(CO_2)_n$ clusters in solid pH_2 which show a complicated pattern of peaks throughout the 2345 to 2350 cm^{-1} region [65].

Finally, the absence of additional features in traces (1a) and (1b), for which the CO_2 is actually an unintentional impurity in samples containing ~ 10 ppm of other dopants, further supports the argument for negligible dopant aggregation under the present sample preparation conditions. Not shown are spectra from other experiments at higher HCl concentrations which *do* show absorption features in the 2346 to 2349 cm^{-1} region attributable to $(HCl)_m(CO_2)_n$ complexes [66]. These 2 to 5 cm^{-1} blue shifts from the matrix isolated monomer absorptions are in line with the +2 cm^{-1} shift reported in previous $HCl/CO_2/Ar$ studies [67,68]. Thus, clustering during deposition to form $(CO_2)_n$ should be even less important for the more dilute 1.2 ppm CO_2 sample depicted in trace (1c).

We thus conclude with confidence that the α, β, and γ features are due to isolated CO_2 molecules. The appearance of *all* detectable absorption features in as-deposited samples within a narrow ≈ 1 cm^{-1} region, especially traces (1c) and (3a), further suggests that even these weaker features may also be due to isolated CO_2 molecules. The new weak features which appear only upon annealing, especially those with significant shifts from the band

center, may be due to $(CO_2)_n$ clusters. We will discuss these possibilities further in the following sections.

4.2. CO_2 molecule trapping site(s)

We attribute the appearance of (at least) three separate absorption peaks for monomeric CO_2 to trapping of CO_2 molecules in multiple trapping sites. Each distinct trapping site by definition corresponds to a different time-averaged structure of dopant and host molecules and so, in principle, can generate a distinct pattern of gas-to-matrix spectral shifts for the dopant vibrational transitions. For purposes of this discussion, we can ascribe the formation of multiple trapping sites during the highly non-equilibrium sample deposition process to (1) imperfections in the underlying host crystal structure, and/or (2) mismatches in the «sizes» of host and guest molecules.

As mentioned in the Introduction, the microscopic structure of our rapid vapor deposited $p\mathrm{H}_2$ solids is far from that of the perfect, single hcp crystals that can be produced by slowly freezing liquid $p\mathrm{H}_2$ [69]. The hcp (*...ABABAB...*) and fcc (*...ABCABCABC...*) structures are only two of the infinite number of densest close-packed structures that can be produced by stacking of close-packed («basal») planes. Patterns with longer repeat units (polytypism), non-periodic structures such as twin and stacking faults, and even random stacked close-packed structures are also possible [70].

Fortunately, the combination of IR and Raman spectroscopies of pure solid $p\mathrm{H}_2$ reveals the symmetries of the sites occupied by the $p\mathrm{H}_2$ molecules [71–74]. We have not detected any vacancy defects in as-deposited undoped $p\mathrm{H}_2$ solids, and have further shown that these samples are not amorphous; rather, they appear to be densest close-packed solids made up of separate hcp and fcc regions [16,22,74]. The introduction of up to ~ 1000 ppm concentrations of dopants like CH_4 and CO, which are nearly the same «size» as a $p\mathrm{H}_2$ molecule in the van der Waals sense, does not significantly affect the $p\mathrm{H}_2$ structure. Thus, trapping of such dopants in single-substitutional vacancies results in the formation of two distinct classes of trapping sites: of D_{3h} symmetry in hcp regions, and O_h symmetry in fcc regions. The experimental $CH_4/p\mathrm{H}_2$ and $CO/p\mathrm{H}_2$ spectra are all consistent with this relatively simple picture [22,38].

However, if our spectroscopic diagnostics are only sensitive to interactions with nearest neighbor $p\mathrm{H}_2$ molecules, then we would necessarily detect *only two* $p\mathrm{H}_2$ environments for *any* arbitrary stacking pattern of basal planes, i.e.: sites in layers ($\underline{B}$) embedded in regions of local hcp stacking (*XAB̲AX*, «hcp-like»), or local fcc stacking (*XAB̲CX*, «fcc-like»). Dopants substituted into hcp-like sites would experience external fields of very nearly D_{3h} symmetry, those in fcc-like sites would exist in nearly octahedral environments. Depending on the particulars of the dopant-$p\mathrm{H}_2$ interactions, the distinction between, for example, «hcp-like» and «true hcp» may be undetectable in a given spectroscopic experiment.

In the case of CO_2 as the dopant, the situation is further complicated by the larger size of CO_2 relative to the $p\mathrm{H}_2$ host. Figure 4 shows this size discrepancy in a semi-quantitative manner, with the CO_2 molecule depicted in single-, double-, and triple-substitutional vacancies in basal planes of spherical $p\mathrm{H}_2$ molecules. Overlap between molecular outlines indicates repulsive interactions, whereas intervening space indicates attractive interactions.

The $p\mathrm{H}_2$ molecules are drawn as circles with diameters representing the 3.8 Å nearest-neighbor separation in solid $p\mathrm{H}_2$ at *l*He temperatures [69]. We use the nearest neighbor separation, instead of the minimum separation for the $p\mathrm{H}_2$–$p\mathrm{H}_2$ interaction potential, to include the effects of quantum zero point motion on the structure of solid $p\mathrm{H}_2$ which would be absent in a simple potential energy minimization. We were unable to find an angle-dependent CO_2–$p\mathrm{H}_2$ interaction potential in the literature, so we resorted to a recently calculated CO_2–He potential instead [75]. Since the minima of the (spherically averaged) He–He, H_2–H_2 , and He–H_2 potentials occur at separations of: 2.94 Å [76], 3.4 Å [69], and 3.4 Å [77], respectively, we expect only minor differences between the length scales of the CO_2–$p\mathrm{H}_2$ and CO_2–He potentials. Subtracting the 1.9 Å effective radius of the $p\mathrm{H}_2$ molecules from the angle dependent minimum of the CO_2–He potential produces the outline of the CO_2 molecule. The «dip» in towards the central C atom indicates the presence of an attrac-

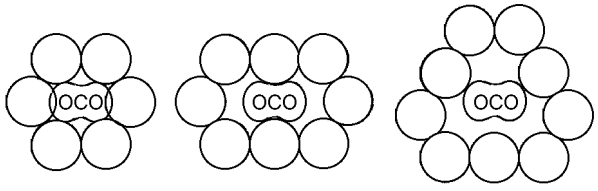

Fig. 4. Hypothetical trapping sites for CO_2 molecules in solid $p\mathrm{H}_2$ based on single-, double-, and triple-substitutional vacancies in close-packed planes of $p\mathrm{H}_2$ molecules.

tive well, and correctly reflects the experimentally determined T-shaped global minimum CO_2–He geometry [78].

Judging from the drawings in Fig. 4, we consider it unlikely, but not impossible, for a CO_2 molecule to occupy a single-substitutional vacancy in solid pH_2 . A relaxed trapping site structure would require considerable distortion of the surrounding pH_2 molecules away from their original lattice positions, leading to numerous smaller repulsive pH_2–pH_2 interactions. On the other hand, the double-substitutional site readily accommodates a CO_2 molecule, and the triple-substitutional site appears perhaps overly spacious.

We can most easily explain our observation of three main peaks in the spectra of as-deposited CO_2/pH_2 solids by trapping of CO_2 molecules in three distinct double-substitutional vacancies. In each case the CO_2 molecules should exist as strongly hindered librators and not as rotors. By comparison with the recent CO_2/N_2 experiments [57], we would expect a single sharp line as the main signature for each trapping site. There is only one type of double-substitutional site in an fcc solid, while there are two different ways of removing two adjacent host molecules in an hcp solid. These are designated «in-plane» (ip) if both host molecules are removed from the same basal plane, and «out-of-plane» (oop) otherwise [79].

Based on their annealing behaviors, we assign the three major lines to CO_2 molecules trapped in double-substitutional sites as follows: the α line to the oop-hcp site, the β line to the ip-hcp site, and the γ line to the fcc site. The virtual disappearance of the γ line upon annealing matches our previous experience with irreversible loss of fcc regions during annealing. We attribute the α line decrease and β line increase upon annealing to the improved alignment of the hcp crystallite c-axis directions with the substrate surface normal. Since our IR beam propagates parallel to this same direction, CO_2 molecules oriented perpendicular to the surface normal will exhibit better alignment of their ν_3 mode transition dipoles with the electric field of the IR beam.

We exclude trapping of CO_2 molecules in triple-substitutional sites because such molecules should exist as slightly hindered rotors. Since the rotational constant of CO_2 is only ≈ 0.4 cm^{-1} , several rotational levels would be populated at the temperatures employed in these experiments. We see no evidence in the spectra for the evenly spaced absorption lines expected for rotational transitions from such levels. We note that our results do not absolutely exclude the possibility of trapping of CO_2 molecules in single-substitutional sites. In analogy to the argument made previously for the double-substitutional sites, one can conceive of two types of relaxed single-substitutional sites in hcp pH_2 which differ in the orientation of the trapped CO_2 molecule with respect to the hcp c-axis.

One final point of comparison is the absorption linewidths expected for the single-vs. double-substitutional trapping sites. In the first case, both ends of the CO_2 molecule would experience strong repulsive interactions with the nearest-neighbor pH_2 molecules, suggesting the likelihood of strong coupling between the CO_2 ν_3 asymmetrical stretching mode and the pH_2 solid. For the double-substitutional site, especially if the center of mass of the CO_2 molecule is strongly localized near the center of the trapping site, the ends of the CO_2 molecule should experience much weaker attractive interactions with those pH_2 nearest-neighbors aligned with the molecular axis. In this case, we would expect very weak coupling of the ν_3 mode with the pH_2 solid, and correspondingly narrow absorption lines.

4.3. Weak absorption features

We turn finally to the origins of the numerous weaker absorption features in the CO_2/pH_2 spectra. Ultimately, successful quantitative modeling of these features should yield the best insights into the CO_2 trapping site structures and librational dynamics, as well as the more general lessons we hope will help us interpret the spectra of larger non-rotating dopant systems. At present, however, we can only offer our qualitative speculations in the form of a list of hypotheses to be examined in the future.

The same multiple trapping site argument used above to explain the α, β, and γ peaks can be extended to include some or all of the peaks observed in the 2343.5 to 2345 cm^{-1} region in as-deposited CO_2/pH_2 samples. In place of double-substitutional sites in hcp and fcc regions we substitute the concepts of hcp-like and fcc-like trapping sites discussed above. In contrast to the CH_4/pH_2 case, for which we found no such distinction, for CO_2/pH_2 subtle differences in final relaxed trapping site structures due to non-nearest-neighbor interactions might induce the $\sim 10\%$ differences in gas-to-matrix shifts required to account for these minor peaks. The irreversible changes observed upon annealing would thus correspond to the disappearance of some of these metastable trapping site structures. The logical extreme of this model, in which each and every line corresponds to the absorption of CO_2 molecules in a particular trapping

site, raises the interesting notion of inhomogeneities as discrete, countable entities; challenging the traditional «continuous» depiction of inhomogeneous broadening.

The extreme dilution of our samples weighs against attributing the weak features in the 2343.5 to 2345 cm^{-1} region to long-range interactions between CO_2 molecules. Vibrational shifts due to resonant interactions between CO_2 molecules die off with increasing separation as R^{-3} [46]; their absolute magnitudes fall below ~ 0.1 cm^{-1} for separations greater than ≈ 20 Å. At a concentration of 1 ppm in solid pH_2 , the number density of CO_2 molecules is only $2.6 \cdot 10^{16}$ cm^{-3}; for a random distribution the mean separation between closest CO_2 molecules is ≈ 200 Å. Furthermore, denoting the distribution of separations between closest CO_2 molecules as $f(R)dR$, then from the peak value near $R = 200$ Å, $f(R)$ tends towards zero as R^2 for decreasing separations. Thus, very few of the CO_2 molecules will be close enough to communicate in this manner. An intriguing mechanism in which dopants interact via the strain fields they induce in the surrounding host lattice has been proposed to explain sharp features in IR absorption spectra of SF_6/Ar matrices [80]. In fact, the spectra reported in that study bear a passing resemblance to our CO_2/pH_2 spectra. However, we find it difficult to accept that such a mechanism could operate over the ~ 100 matrix host diameters intervening between CO_2 dopants in our 1 ppm samples.

The models proposed so far in this section cannot explain the observed *reversible* temperature dependent changes to the spectra. Several of the weaker features appear to originate from thermally populated initial states. On the other hand, the α″ line appears to originate from a very easily thermally de-populated initial state; we estimate that the height of the α″ peak decreases $\approx$ 50-fold upon warming from $T = 2.4$ to 4.8 K. Since the lowest lying vibrational state of a gas-phase CO_2 molecule is the ν_2 bending mode at 667 cm^{-1}, these thermally populated states must involve interactions with the pH_2 solid, although we can as yet offer no specifics as to the libration-translation dynamics involved.

Another possibility is the aggregation of oH_2 impurities around the CO_2 molecules. Assuming complete equilibration in our ortho/para converter [17] at $T = 15$ K, the residual oH_2 concentration is ≈ 100 ppm. Actually, assuming natural isotopic abundance, the pH_2 solids should also contain ≈ 300 ppm HD molecules, but HD molecules are immobilized in the solid at *l*He temperatures. On the other hand, the $J = 1$ «ortho» excitations are mobile by a process known as «quantum diffusion», i.e.: the conversion of adjacent oH_2–pH_2 pairs into pH_2–oH_2 pairs [69,73,81,82]. Any $J = 1$ excitation that diffuses into the vicinity of a trapped CO_2 molecule would localize to form an oH_2–CO_2 pair bound together via the electric quadrupole-quadrupole (EQQ) interaction. Based on previously published $HD/oH_2/pH_2$ and $D_2/oH_2/pH_2$ spectra [4,5], this same EQQ interaction should be capable of producing complex features over a ~ 1 cm^{-1} region of the CO_2 spectrum. In this picture, the reversible temperature dependent spectral changes could be attributed to absorptions involving different «orientational» states of the oH_2 molecules, rather than the libration-translation dynamics of the CO_2 molecules.

Given the present data, we can only note in passing that the weak features in the 2345 to 2348 cm^{-1} region shown in Fig. 3 which grow in upon annealing show blue-shifts relative to the α and β peaks consistent with clustering of a small fraction of the CO_2 molecules to form CO_2 dimers and trimers.

5. Conclusions and future directions

We report high resolution IR absorption spectra of CO_2 molecules isolated in rapid vapor deposited pH_2 solids. The absence of a regularly spaced progression of lines is taken as evidence that the CO_2 molecules cannot rotate, and instead exist as strongly hindered librators. The three main absorption features are assigned to CO_2 molecules trapped in double-substitutional sites in hcp and fcc regions of the as-deposited solids. Numerous weaker spectral features remain unexplained. Reversible temperature dependent intensities demonstrate that some of these weaker transitions originate from low-lying thermally populated states. Some of the 2 to 5 cm^{-1} blue-shifted weak features observed upon annealing of the samples may be due to small $(CO_2)_n$ clusters.

We are preparing to perform a new series of experiments on CO_2/pH_2 samples, including the use of isotopically substituted CO_2 molecules. Breaking the inversion symmetry of the CO_2 molecule by trapping the $^{16}O^{12}C^{18}O$ isotopomer will alter the nature of the allowed librational states. Trapping gradually increasing concentrations of CO_2 molecules should permit the identification of spectral features due to dimers and larger clusters. Manipulating the residual oH_2 concentration by varying the ortho/para converter temperature should clarify the importance of oH_2–CO_2 clustering.

We expect that quantum simulation techniques will be very valuable in elucidating the trapping site structures and librational dynamics of the CO_2/pH_2 system, as demonstrated previously for O_2 doped hydrogen solids [83–86].

Acknowledgements

We thank the authors of Refs. 57 and 65 for advance copies of their manuscripts. We thank the referee for pointing out a serious error in our original discussion of the temperature dependence of the α'' peak.

1. M. Okumura, M. C. Chan, and T. Oka, *Phys. Rev. Lett.* **62**, 32 (1989).
2. T. Oka, *Annu. Rev. Phys. Chem.* **44**, 299 (1993).
3. T. Oka, *Fiz. Nizk. Temp.* **22**, 134 (1996) [*Low Temp. Phys.* **22**, 96 (1996)].
4. D. P. Weliky, K. E. Kerr, T. J. Byers, Y. Zhang, T. Momose, and T. Oka, *J. Chem. Phys.* **105**, 4461 (1996).
5. Y. Zhang, T. J. Byers, M. C. Chan, T. Momose, K. E. Kerr, D. P. Weliky, and T. Oka, *Phys. Rev.* **B58**, 218 (1998).
6. T. Momose, *J. Chem. Phys.* **107**, 7695 (1997).
7. T. Momose, M. Miki, T. Wakabayashi, T. Shida, M. C. Chan, S. S. Lee, and T. Oka, *J. Chem. Phys.* **107**, 7707 (1997).
8. T. Momose, H. Katsuki, H. Hoshina, N. Sogoshi, T. Wakabayashi, and T. Shida, *J. Chem. Phys.* **107**, 7717 (1997).
9. T. Momose and T. Shida, *Bull. Chem. Soc. Jpn.* **71**, 1 (1998).
10. H. Hoshina, T. Wakabayashi, T. Momose, and T. Shida, *J. Chem. Phys.* **110**, 5728 (1999).
11. R. Steinhoff, K. V. S. R. Apparao, D. W. Ferguson, K. N. Rao, B. P. Winnewisser, and M. Winnewisser, *Appl. Opt.* **32**, 6577 (1993).
12. R. Steinhoff, K. V. S. R. Apparao, D. W. Ferguson, K. N. Rao, B. P. Winnewisser, and M. Winnewisser, *Can. J. Phys.* **72**, 1122 (1994).
13. M. Mengel, B. P. Winnewisser, and M. Winnewisser, *Phys. Rev.* **B55**, 10420 (1997).
14. M. Mengel, B. P. Winnewisser, and M. Winnewisser, *J. Mol. Spectr.* **188**, 221 (1998).
15. *Proceedings of the High Energy Density Matter (HEDM) Contractors' Conference held 17–20 May 1998 in Monterey*, CA, M.R. Berman (ed.), U.S. Air Force Office of Scientific Research, Arlington, VA (1999).
16. M. E. Fajardo and S. Tam, *J. Chem. Phys.* **108**, 4237 (1998).
17. S. Tam and M. E. Fajardo, *Rev. Sci. Instrum.* **70**, 1926 (1999).
18. P. C. Souers, *Hydrogen Properties for Fusion Energy*, Univ. of California Press, Berkeley (1986).
19. M. E. Fajardo, *J. Chem. Phys.* **98**, 110 (1993).
20. M. E. Fajardo, S. Tam, T. L. Thompson, and M. E. Cordonnier, *Chem. Phys.* **189**, 351 (1994).
21. S. Tam, M. Macler, and M. E. Fajardo, *J. Chem. Phys.* **106**, 8955 (1997).
22. S. Tam, M. E. Fajardo, H. Katsuki, H. Hoshina, T. Wakabayashi, and T. Momose, *J. Chem. Phys.* **108**, 4237 (1998).
23. L. Pauling, *Phys. Rev.* **36**, 430 (1930).
24. A. F. Devonshire, *Proc. Roy. Soc. (London)* **A153**, 601 (1936).
25. W. H. Flygare, *J. Chem. Phys.* **39**, 2263 (1963).
26. H. F. King and D. F. Hornig, *J. Chem. Phys.* **44**, 4520 (1966).
27. R. E. Miller and J. C. Decius, *J. Chem. Phys.* **59**, 4871 (1973).
28. H. Friedmann and S. Kimel, *J. Chem. Phys.* **43**, 3925 (1965).
29. M. T. Bowers, G. I. Kerley, and W. H. Flygare, *J. Chem. Phys.* **45**, 3399 (1966).
30. H. Friedmann and S. Kimel, *J. Chem. Phys.* **47**, 3589 (1967).
31. H. Friedmann, A. Shalom, and S. Kimel, *J. Chem. Phys.* **50**, 2496 (1969).
32. P. D. Mannheim, *Phys. Rev.* **B5**, 745 (1972).
33. P. D. Mannheim, *J. Chem. Phys.* **56**, 1006 (1972).
34. J. Manz, *J. Am. Chem. Soc.* **102**, 1801 (1980).
35. M. Allavena, H. Chakroun, and D. White, *J. Chem. Phys.* **77**, 1757 (1982).
36. H. Kono and S.H. Lin, *J. Chem. Phys.* **78**, 2607 (1983).
37. I. L. Garzon and E. Blaisten-Barojas, *J. Chem. Phys.* **83**, 4311 (1985).
38. M. E. Fajardo, S. Tam, and T. Momose, unpublished.
39. *Molecular Spectroscopy: Modern Research Volume III*, K. N. Rao (ed.), Academic Press, New York (1985).
40. G. Guelachvili and K. N. Rao, *Hanbook of Infrared Standards*, Academic Press, New York (1985).
41. G. Guelachvili et al., *Spectrochimica Acta Part* **A52**, 717 (1996).
42. M. A. Walsh, T. H. England, T. R. Dyke, and B. J. Howard, *Chem. Phys. Lett.* **142**, 265 (1987).
43. R. Eggenberger, S. Gerber, and H. Huber, *Mol. Phys.* **72**, 433 (1991).
44. Z. Slanina, S. J. Kim, and K. Fox, *Vibrational Spectroscopy* **4**, 251 (1993).
45. L. M. Nxumalo, T. A. Ford, and A. J. Cox, *J. Mol. Struct. (Theochem.)* **307**, 153 (1994).
46. M. J. Weida, J. M. Sperhac, and D. J. Nesbitt, *J. Chem. Phys.* **103**, 7685 (1995).
47. M. J. Weida and D. J. Nesbitt, *J. Chem. Phys.* **105**, 10210 (1996).
48. J. A. Barnes and T. E. Gough, *J. Chem. Phys.* **86**, 6012 (1987).
49. G. E. Ewing and D. T. Sheng, *J. Phys. Chem.* **92**, 4063 (1988).
50. W. E. Osberg and D. F. Hornig, *J. Chem. Phys.* **20**, 1345 (1952).
51. B. E. Wood and J. A. Roux, *J. Opt. Soc. Am.* **72**, 720 (1982).
52. M. Falk, *J. Chem. Phys.* **86**, 560 (1987).
53. M. A. Ovchinnikov and C. A. Wight, *J. Chem. Phys.* **99**, 3374 (1993).
54. *Vibrational Spectroscopy of Trapped Species*, H. E. Hallam (ed.), Wiley, London (1973).
55. D. W. Ball, Z. H. Kafafi, L. Fredin, R. H. Hauge, and J. L. Margrave, *A Bibliography of Matrix Isolation Spectroscopy: 1954–1985*, Rice U. Press, Houston, TX (1988).
56. D. W. Ochsner, D. W. Ball, and Z. H. Kafafi, A *Bibliography of Matrix Isolation Spectroscopy: 1985–1997*, U.S. Naval Research Laboratory, Washington, DC (1998).
57. M. Vetter, A. P. Brodyanski, and H. J. Jodl, *J. Phys. Chem.* **A104**, 3698 (2000).
58. L. Fredin, B. Nelander, and G. Ribbegard, *J. Mol. Spectr.* **53**, 410 (1974).

59. R. Guasti, V. Schettino, and N. Brigot, *Chem. Phys.* **34**, 391 (1978).
60. L. M. Nxumalo and T. A. Ford, *J. Mol. Spectr.* **327**, 145 (1994).
61. Y. Ogawara, A. Bruneau, and T. Kimura, *Anal. Chem.* **66**, 4354 (1994).
62. E. Knozinger and P. Beichert, *J. Phys. Chem.* **99**, 4906 (1995).
63. M. J. Irvine and A. D. E. Pullin, *Aust. J. Chem.* **35**, 1961 (1982).
64. M. J. Irvine and A. D. E. Pullin, *Spectrochimica Acta* **43A**, 611 (1987).
65. M. Fushitani, T. Shida, T. Momose, and M. Rasanen, *J. Phys. Chem.* **A104**, 3635 (2000).
66. M. E. Fajardo and S. Tam, unpublished.
67. L. Andrews, R. T. Arlinghaus, and G. L. Johnson, *J. Chem. Phys.* **78**, 6353 (1983).
68. N. Fourati, B. Silvi, and J. P. Perchard, *J. Chem. Phys.* **81**, 4737 (1984).
69. I. F. Silvera, *Rev. Mod. Phys.* **52**, 393 (1980).
70. C. Kittel, *Introduction to Solid State Physics 6th Edition*, Wiley, New York (1986).
71. J. Van Kranendonk and H. P. Gush, *Phys. Lett.* **1**, 22 (1962).
72. J. Van Kranendonk and G. Karl, *Rev. Mod. Phys.* **40**, 531 (1968).
73. J. Van Kranendonk, *Solid Hydrogen: Theory of the Properties of Solid* H_2, HD, and D_2, Plenum Press, New York (1983).
74. G. W. Collins, W. G. Unites, E. R. Mapoles, and T. P. Bernat, *Phys. Rev.* **B53**, 102 (1996).
75. G. Yan, M. Yang, D. Xie, *J. Chem. Phys.* **109**, 10284 (1998).
76. J. B. Anderson, C. A. Traynor, and B. M. Boghosian, *J. Chem. Phys.* **99**, 345 (1993).
77. W. R. Rodwell and G. Scoles, *J. Phys. Chem.* **86**, 1053 (1982).
78. M. J. Weida, J. M. Sperhac, D. J. Nesbitt, and J. M. Hutson, *J. Chem. Phys.* **101**, 8351 (1994).
79. A. B. Harris, A. J. Berlinsky, and W. N. Hardy, *Can. J. Phys.* **55**, 1180 (1977).
80. D. Hallamasek, E. Babka, and E. Knozinger, *J. Mol. Struct.* **408/409**, 125 (1997).
81. L. I. Amstutz, J. R. Thompson, and H. Meyer, *Phys. Rev. Lett.* **21**, 1175 (1968).
82. R. Oyarzun and J. Van Kranendonk, *Phys. Rev. Lett.* **26**, 646 (1971).
83. A. V. Danilychev, V. E. Bondybey, V. A. Apkarian, S. Tanaka, H. Kajihara, and S. Koda, *J. Chem. Phys.* **103**, 4292 (1995).
84. M. Sterling, Z. Li, and V.A. Apkarian, *J. Chem. Phys.* **103**, 5679 (1995).
85. Z. Li, V. A. Apkarian, and L. B. Harding, *J. Chem. Phys.* **106**, 942 (1997).
86. Z. Li and V. A. Apkarian, *J. Chem. Phys.* **107**, 1544 (1997).